Lithium as a proxy for Silicate Weathering during the Southeast Asian Monsoon

Author: Martha Longley

Advisor: Noah Planavsky

Second Reader: Ryan McKenzie

May 2, 2018

A Senior Thesis presented to the faculty of the Department of Geology and Geophysics, Yale University, in partial fulfillment of the Bachelor's Degree.

ABSTRACT

Lithium (Li), which displays large isotope fractionations during secondary clay formation, is the only weathering tracer that is approximately uniformly distributed throughout the Earth's crust. Additionally, Li is hosted almost exclusively in silicate minerals, which makes it a useful proxy for silicate weathering as opposed to chemical denudation more broadly. As such, Li has been used extensively to track changes in silicate weathering and the tectonic factors controlling Earth's climate. However, there are aspects of the modern Li cycle that are poorly constrained, leading to uncertainties in the use of Li isotopes as paleo-weathering proxies. Foremost, in modern tropical settings with high rates of chemical weathering, there remains a poor understanding of the dominant factors controlling Li isotope fractionation. The behavior of Li in tropical weathering regimes that experience large seasonal swings in precipitation has not previously been characterized — even though these regimes are likely to make large contributions to global Li mass balance and carbon dioxide removal. In this study, we collected river water samples in Thailand during the monsoon season. Lithium concentrations ranged from 0.024 μM to 0.788 μM. The average concentration was 0.140 μM (n = 67) which is lower than the global average of 0.32 μM. There was an increase in mean δ^7Li associated with river size, with the largest rivers having a mean δ^7Li of 28.55‰ — which departs significantly from the global average of 23‰ (Li and West 2014). The presence of anomalously positive δ^7Li may be caused by individual clay minerals or multiple episodes of clay formation tied to the wet and dry cycles characteristic of the Southeast Asian Monsoon. Further, these results confirm our hypothesis that in Thailand, neither Li concentrations nor δ^7Li are controlled by bedrock lithology or elevation. More broadly, these results support the view that intensive weathering will not necessarily mute Li fractionations during terrestrial weathering as was previously expected based on Li isotope values in the Amazon River Basin.

INTRODUCTION

Weathering of silicate rocks, which consumes carbon dioxide, is an important regulator of climate and seawater chemistry on million year timescales (Walker et al. 1981 and Berner et al. 1983). It follows that quantifying variation in silicate weathering is a critical step in understanding the degree to which tectonic processes have impacted climate throughout Earth's history. Though the stoichiometry of individual weathering reactions depend on silicate mineralogy, the following generalized equation illustrates the chemical basis of carbon dioxide

consumption:

$$CaSiO_3 + CO_2 \rightarrow CaCO_3 + SiO_2$$

with magnesium often substituting in for calcium (Urey 1952). The rate of the silicate weathering reaction is determined by four main parameters. First, tectonic uplift controls the supply of silicate minerals by exposing the surface area necessary for the reaction to proceed. Second, precipitation limits the extent of the reaction, which occurs in aqueous conditions. Third, low pH, due to vegetation-derived corrosive organic acids, increases the reaction rate of silicate weathering by helping to break down the minerals of interest (Brady and Carroll 1994). Lastly, as with all chemical reactions, temperature has a positive association with reaction rate as it raises the proportion of molecules with sufficient energy to react upon collision according to the Maxwell-Boltzman distribution (Boltzmann 1884, Maxwell 1860). Consistent with this view of silicate reaction parameters, precipitation is positively associated with increased breakdown of silicate minerals (Brady et al. 1999). Likewise, experimental results show that silicate weathering is sensitive to changes in temperature. For instance, a four-fold increase in reaction rate has been observed as temperature increased from 14°C to 26°C (Brady and Carroll 1994). However, in large field studies the effects of these parameters on silicate weathering rates have been less clear (Gaillardet et al. 1999).

Establishing ways to track silicate weathering is essential to move forward our understanding of Cenozoic climate change. As the most recent geologic period, the Cenozoic is arguably the best era for modeling modern climate. Cenozoic records of climate variables generally exist at much higher resolution than records from earlier eras. Additionally, the Cenozoic is marked by a hothouse climate during the Paleocene-Eocene Thermal Maximum (PETM) at ~55 Ma, which has the highest recorded temperatures of the past 65 million years (Zachos et al. 2001, 2005). This period is of particular relevance today because the dramatic increase in temperature was the result of an abrupt rise in atmospheric carbon dioxide concentrations (Zachos et al. 2001, 2005). Though this abrupt temperature rise was much slower than modern global warming, it is one of the best analogues for modern day climate change. Thus understanding how and why climate changed through the PETM is essential to inform our predictions of the impact of anthropogenic carbon emissions on Earth's climate in the coming years.

Misra and Froelich (2012) suggest that high carbon dioxide concentrations were able to persist during the PETM because of depressed silicate weathering due to slow continental uplift. However, there is no geomorphological evidence for or against slow uplift rates from 65 Ma to 45 Ma. While there is geomorphological evidence of mountain-building from 40 Ma to present, which corresponds to a steady decrease in carbon dioxide concentrations and mean oceanic temperature, constraints on silicate weathering are necessary in order to quantify the degree to which this uplift can explain the observed drop in carbon dioxide. To explore this question, Misra and Froelich (2012) use strontium (Sr), osmium (Os) and Li behavior to infer physical weathering dynamics from continental inputs. These three trace metals are all liberated from bedrock during weathering processes and eventually input into the ocean. Fractionation during dissolution of Os and Sr is negligible and as a result, the riverine input is reflective of bedrock composition. In both Os and Sr, the ratio between radioactive and stable isotopes is much higher in differentiated continental rocks than it is in oceanfloor basalts, due to the incompatibility of the radioactive parent isotopes (rubidium-87 and osmium-187, respectively) in ultramafic minerals. Thus changes in the ratios of radioactive to stable Sr and Os in seawater can loosely track continental weathering fluxes. With regards to Cenozoic cooling, there is a steady rise in $^{87}Sr/^{86}Sr$ and $^{187}Os/^{186}Os$ that matches decreasing atmospheric pCO_2 (Hodell et al. 1991, Peucker-Ehrenbrink 2002). However, direct silicate weathering flux cannot be estimated from strontium and osmium records because these elements are not uniformly distributed throughout the Earth's crust. Weathering of highly concentrated, ^{87}Sr-enriched carbonates and ^{187}Os-enriched shales can drown out isotopic signals due to silicate weathering, making it impossible to infer carbon dioxide consumption from these records (Huh & Edmond 1998 and Ravizza & Esser 1993).

In contrast, Li isotopes have the potential to directly track silicate weathering, given that 95% of lithium resides in silicate minerals, and Li distribution is roughly constant throughout the Earth's crust (Aller 2014). Changes in the δ^7Li composition of seawater have been tied to silicate weathering processes specifically, arguably making the isotope system a more useful tracer of carbon dioxide removal than traditional (Os and Sr) weathering proxies (Pistiner and Henderson 2003).

Lithium isotopic fractionations are described using delta notation:

$$\delta^7Li(‰) = [(^7Li/^6Li)_{sample} / (^7Li/^6Li)_{L\text{-}SVEC} - 1] \times 10^3$$

where the isotopic composition of NIST L-SVEC is 12.02+/– 0.03‰, the isotopic composition of bedrock is 0-1‰, and the terrestrial fractionation range is generally –20-40‰ (Tang et al. 2007). As an alkali metal, Li rarely has its s-orbital electron, meaning it has a valence state of +1 and it is therefore not fractionated by redox conditions. Additionally, it is not meaningfully fractionated during biological processes (Schmitt et al. 2012). This makes it broadly applicable throughout Earth's history, despite changes in biological activity and ocean oxidation state.

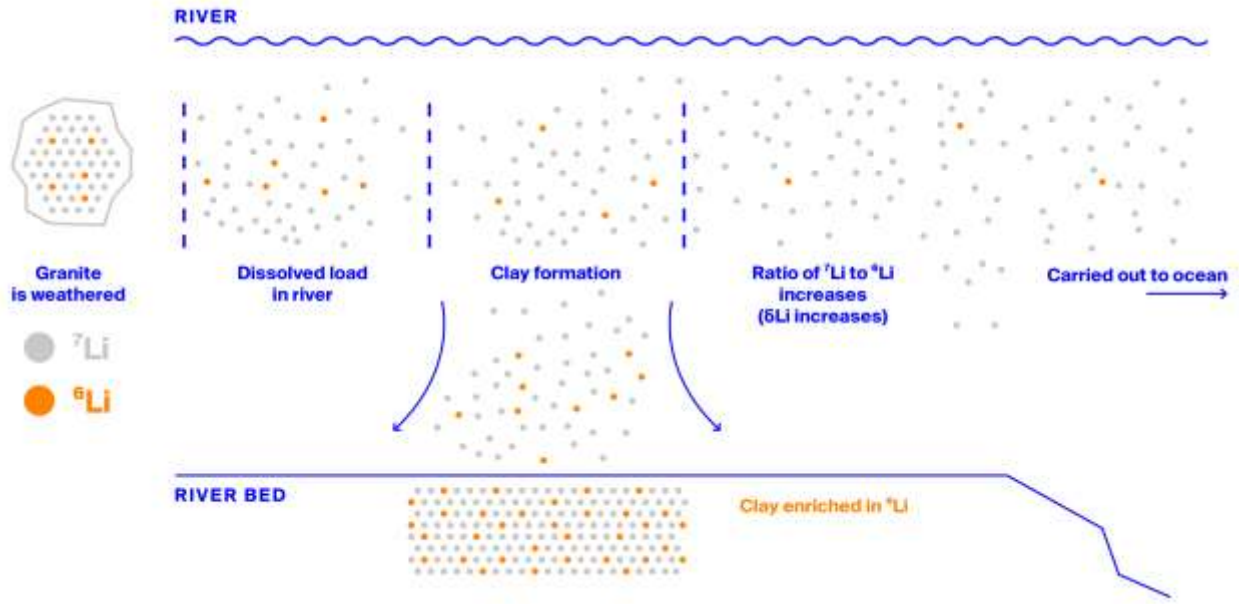

Figure 1: Illustration of ^7Li enrichment of the dissolved load during clay formation.

Lithium tracks silicate weathering intensity, defined here as chemical silicate weathering (flux of silicate-derived dissolved load) relative to denudation rate. This can be tracked in low-temperature systems because during incongruent weathering, wherein secondary clays form, ^6Li is preferentially retained in clay minerals (Pistiner & Henderson 2003, Huh et al. 1998). This occurs because hydrated Li has a very similar radius to magnesium, and is easily substituted into clay matrices. The likelihood of Li substitution increases as clay formation rates increase, making it an indicator not only of the total amount of clay formation, but the rate at which it occurred. ^6Li is preferentially incorporated into clays as they form because it has a lower mass and thus has a higher bond energy:

$$E_i = \left(n + \frac{1}{2}\right) hv$$

where h is Planck's constant, n is the quantum number and v is the vibrational energy. Since vibrational energy is an inverse function of mass:

$$v = \frac{1}{2\pi}\sqrt{\frac{\kappa}{\mu}}$$

where κ is a constant and μ is the reduced mass, bond energy increases as mass decreases. Since ^{6}Li has a greater bond energy, there is a smaller difference between the energy of dissociation and the bond energy. This means that the barrier energy necessary for it to react with the clay matrix is lower for ^{6}Li than it is for ^{7}Li. Since this reaction does not proceed to equilibrium, lithium incorporation into clays leaves surrounding waters enriched in ^{7}Li. These enriched river waters then have the capacity to change the chemical composition of the ocean, which is recorded in carbonates. Since the residence time of Li is approximately 1.2 Ma, we can assume that lithium is well mixed given ocean mixing rates on the order of 1000 years (Li and West 2014). Though source rock δ^{7}Li can vary slightly and thus can have small effects on dissolved Li composition, the dissolution process does not cause any fractionation (e.g., Wang et al. 2014, Pistiner & Henderson 2003).

The Li-isotope budget is controlled by four main factors: riverine flux, hydrothermal flux and removal through "reverse weathering" primarily divided into basalt alteration and sediment uptake (Li and West 2014). In modeling these four levers, Li and West (2014) could not reproduce the Cenozoic change in Li isotopes from 23‰ in 60 Ma to 31‰ in the modern without changing riverine δ^{7}Li inputs (Li and West 2014). However, Li fractionation factors remain poorly understood, making it difficult to infer what continental conditions would lead to this dramatic rise in δ^{7}Li. An important step in improving our understanding of Li fractionation factors is to document Li behavior in a wide range of geologic contexts. Existing models are built upon data from a few select regions, namely, Congo, the Ganges Alluvial Plane, the Amazon River Basin, Iceland, New Zealand and the Mackenzie River basin in Canada. Many of these regions are at temperate, subarctic or arctic latitudes, meaning they are not likely to be representative of regimes making large contributions to seawater chemistry or chemical

denudation rates. Absent from this record is data on lithium behavior in Southeast Asia, where a significant portion of global silicate weathering occurs (Hartmann et al. 2014).

Even in the limited number of regions for which we have data on Li, the relationship between δ^7Li and silicate weathering rates is highly variable. For instance, in Iceland, areas with the highest weathering rates and the most recently deposited basalts have the lowest δ^7Li values, and Li isotopic composition of the dissolved load can be expressed as a function of weathering rate using the equation: $\delta^7\text{Li} = -4.8(+/-1.8)\ln(w) + 36(+/-5.9)$ where w is the chemical silicate erosion rate (Vigier et al. 2009). However, this mathematical relationship did not hold in other regions — a study on the Mackenzie River Basin, a mixed-lithology Canadian basin, found that while δ^7Li did decrease as weathering rates increased, δ^7Li was not a function of chemical denudation rate (Millot et al. 2010). In this region, areas of uplift were associated with the highest δ^7Li values, while floodplains exhibited low δ^7Li and high weathering rates. By contrast, in the Ganges Alluvial Plain, which accounts for 3% of total riverine input, δ^7Li values were lowest in areas of uplift, with the flood plain δ^7Li higher and markedly steady beginning 500 meters from the main frontal thrust (Pogge von Strandmann et al. 2017). This trend was matched in both the Changjiang main channel and the Congo River mouth, where δ^7Li values increased from high elevation to low elevation (Wang et al. 2014 and Henchiri et al. 2016). In New Zealand, uplift rate specifically was inversely correlated with δ^7Li values (Pogge von Strandmann et al. 2015).

These conflicting results complicate interpretations that δ^7Li represents simply uplift or absence of uplift. However, they do not necessarily contradict one another. Highly congruent systems can occur either in kinetically-limited mountain belts or in transport limited lowlands that have weathering conditions necessary for the re-dissolution of secondary clays. For instance, in the Amazon, both congruent and incongruent weathering were observed in floodplains — incongruent weathering occurred in lowlands with extensive secondary clay formation while congruent weathering occurred in lowlands that had secondary clay formation coupled with organic-matter facilitated dissolution (Dellinger et al. 2015). These variable relationships highlight the need for a more nuanced understanding of lithium isotopes that accounts for geomorphological and climatological differences in weathering regimes.

There is currently a dearth of δ^7Li records from Southeast Asia, a region analogous to those we would expect to have high rates of silicate weathering and to contribute substantially to the global Li mass balance in the past. Southeast Asia is characterized by uplift in the north, high rates of precipitation during the summer monsoon, warm temperatures and abundant vegetation. This may be analogous to the African and Indian continents, which moved progressively upward into the Intertropical Convergence Zone throughout the Cenozoic (van Hinsbergen et al. 2012). Here we report 89 δ^7Li values of the dissolved load from rivers across Thailand during the monsoon season. In many of our samples, δ^7Li was much more positive than the values measured in other parts of the world. This suggests that the Southeast Asian Monsoon season weather patterns — defined by wet and dry cycles on an order of magnitude of several days — may lead to multiple clay formation events and markedly positive δ^7Li inputs. In addition, the mean δ^7Li of large rivers, which are the rivers most likely to alter seawater chemistry, were significantly greater than those found in other regions of the world — which highlights the need to revisit estimates of global lithium isotope inputs from rivers (e.g., Dellinger 2015, Li and West 2014).

STUDY AREA

Thailand is covered by tropical rainforest. It experiences a monsoon season, which peaks in precipitation during August and September. These samples were collected in the month of August, which has, on average, 200 mm of precipitation. During sample collection, precipitation was marked by 1-3 day long periods of little to no precipitation followed by heavy precipitation, often punctuated with downpour strong enough to cause flooding. Average temperature from sample collection was 27°C. The average pH of waters in our samples was 7.3, and ranged from 6-8.5. Aside from weather conditions, Thailand was selected because it allows for lithological controls. Most age groups sampled were sampled at both high and low elevation. In addition, the current uplift in northwest Thailand allows for the sampling of a wide range of bedrock types across constant elevation and biological conditions. Samples were taken from a range of consecutive river orders to determine if riverine isotopic composition was conserved. This was to address conflicting evidence of lithium isotope conservation across river confluences. Measurements from the Amazon basin have suggested that at the mouth of a river, which is most

relevant to constraining seawater inputs, the lithium isotopic composition may be more reflective of floodplain processes than a conservative sum of the its tributaries (Dellinger et al. 2015). However, in the Congo River Basin, a 14-22‰ range of δ^7Li at the mouth that corresponded to tributary input values suggests that lithium can be a conservative tracer (Henrichi et al. 2016). We define four main regions:

1. ***Phetchabun Mountains***

The Phetchabun mountains are located in central Thailand. Elevation of samples in this region ranged from 188 – 677 m. The lithology of higher elevation sample sites was Cretaceous-era sandstone, siltstone and conglomerates. Lower elevation samples were from regions with Quaternary fluvial deposits. Rivers drained into the Pa Sak River, which drains into the Chao Phraya and has an annual discharge of rate of 76.04 m^3/s, representing 8.2% of the Chao Phraya's discharge rate (Thai Meteorological Department).

2. ***Khorat Plateau***

The Khorat Plateau lies to the east of the Phetchabun mountains. Samples from this region flow through the Maha Sarakham Formation, which is composed of siltstone, claystone, sandstone, rock salt and gypsum from the Cretaceous period. The average elevation of samples collected in this area was 200 m. Rivers sampled eventually drained into the Mekong River, which runs along the northeast boarder of Thailand and into the South China Sea. The Mekong has an average discharge rate of 1920.92 $m^3s^{-`}$ during the month of August (Wisconsin Hydrological Institute).

3. ***Thai Highlands***

The Thai Highlands are an active area of uplift in the northwest corner of Thailand. They are further subdivided into two categories.

Eastern Thai Highlands:

The Eastern Thai Highlands extend from the Luang Prabang Range on the border of Laos to the Phi Pan Nam Mountains below Chiang Rai. Samples collected in the eastern half drain into the Nan River, while samples collected in the western half drain into the Yom River. The Nan and

Yom join in Nakhon Sawan to form the Chao Phraya. Jurassic- and Triassic-era sedimentary rocks dominate this region, including shales, siltstone, mudstone, sandstone, limestone, chert and conglomerates. Relief in this region ranges from 200-2000 m. Sample elevation ranged from 48 to 883 m, with the mean elevation around 340 m.

Western Thai Highlands:

The Western Thai Highlands are composed of the Luang Prabang Range and the Dawna Range. The bedrock lithology varies, but source rock generally includes conglomerate, shale, chert and limestone from the Permian, Devonian, and Carboniferous periods along with granites from the Cretaceous-Carboniferous periods. Relief ranged from 200-2000 m. Rivers in this region flow into the Salween River and eventually into the Andaman Sea. The Salween River has an annual discharge of 678.6 m^3s^{-1}.

4. Lowlands

The lowlands have elevation below 200 m, and occupy south-central Thailand. The dominant lithology in this region is Quaternary fluvial deposits. Samples in this region were mainly collected from the Chao Phraya and its tributaries. The catchment area of the upper Chao Phraya is 104,481 km^2 (Jamrussi & Toda 2017). The Chao Phraya has an average annual discharge of 139.48 m^3s^{-1} (Wisconsin Hydrological Institute). August has one of the highest monthly discharge rates, at 924.78 m^3s^{-1}, which is 200 m^3s^{-1} above the average monthly discharge rate.

SAMPLING AND CONCENTRATION METHODS

River samples were collected between August 1 and August 22, 2017. Samples were collected in a vinyl-coated nylon bucket and filtered 1-4 hours after collection using acetate cellulose filters, 0.2 μm. They were stored in sterile polypropylene tubes. For concentration measurements, 4 grams of river water was evaporated at 90°C and the remaining residue was digested with 1 mL 16 N distilled nitric acid and 3 mL 11 N distilled hydrochloric acid. The samples were reconstituted in 2 mL 5% nitric acid with 2 ppb indium as an internal standard and run on Thermo Finnegan Element XR ICP-MS. Each lithium measurement was calibrated by multiplying the intensity of lithium by the intensity of indium in the sample divided by the intensity of indium in the blank and subtracting the intensity of lithium in the blank from this

normalized value. Concentration was then calculated by multiplying the lithium intensity by the average slope of lithium concentration versus lithium intensity calibration curves from before and after the sample measurement and adding the average y-intercept. Duplicate samples were measured with 5% precision. A diluted seawater (OSIL, salinity 35.0 +/– 0.2% PSU 26/08/2015) was run alongside the samples and the measured concentrations were within 5% accuracy of previously documented seawater lithium concentrations.

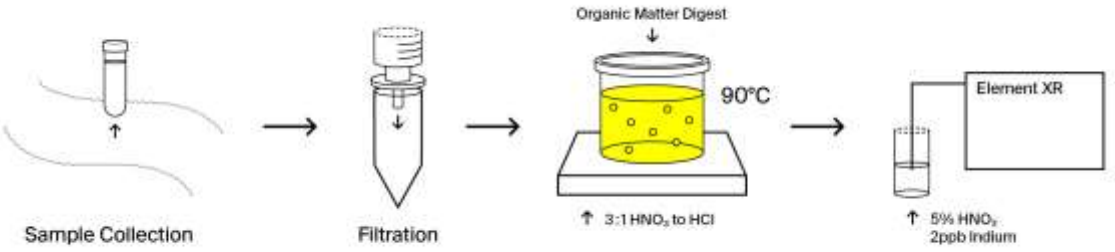

Figure 2: Methods for Sample Collection and Concentration Measurements

LI ISOTOPE MEASUREMENTS

River samples with 25 ng lithium were first evaporated and digested in 1 mL 16 N distilled nitric acid and 3 mL 11 N distilled hydrochloric acid. Next, lithium was separated from other elements. This is an important component of the isotope measurements since contamination from other elements can reduce ionization efficiency, which in turn can lead to fractionation during isotope measurements. Specifically, high levels of sodium have been shown to interfere with ionization and cause isotopic fractionation in Inductively Coupled Plasma Mass Spectrometers (ICP-MS), (Grégoire et al. 1996) the instrument used to measure isotopic composition samples in this study. Additionally, there is Li isotope fractionation during ion-exchange chromatography — ^{7}Li passes more readily through cation-exchange resin than ^{6}Li. Thus it is important that 100% of lithium is recovered during column chromatography, in order to ensure no fractionation is preserved in samples after separation from sodium. In this study, three well-measured standards, seawater (OSIL, salinity 35.0 +/– 0.2% PSU 26/08/2015), L-SVEC and BHVO were run alongside

samples to ensure that no fractionation was occurred during column chromatography or during measurement (Taylor & Urey 1938, Oi et al. 1997, Moriguti & Nakamura 1998). Blanks were also run to ensure samples were not contaminated during preparation.

Ion-exchange chromatography was conducted according to the following procedure, adapted from James and Palmer (2000), modified for 25 ng of lithium. Columns with 2.7 mL of organic cation-exchange resin — styrene-divinylbenzene cross-linked copolymer with sulfonic acid functional groups (Bio-Rad AG50-X12) — were washed by passing through 10 mL 6N hydrochloric acid (distilled), followed by 10 mL deionized water, followed by 10 mL 6N hydrochloric acid (distilled) followed by 10 mL deionized water. Columns were then conditioned using 5 mL 0.200 N hydrochloric acid (distilled). The digested sample, reconstituted in 1 mL 0.200 N hydrochloric acid (distilled), was loaded onto the columns. Though Li is the smallest of the alkali elements, it has the largest hydrated radius and thus has the lowest affinity for the cation exchange resin. Thus after passing through 16 mL 0.200 N hydrochloric acid in four steps (1 mL, 1 mL, 7 mL, 7 mL) lithium was eluted using 24 mL 0.200 N hydrochloric acid in four volumes of 6 mL. In theory, sodium, which has a smaller hydrated radius and thus a higher affinity for the cation-exchange resin, remains on the resin. Sodium is removed during the wash procedure which uses highly concentrated hydrochloric acid to remove all of the alkali metals.

The eluent was dried down on hot plates at 90°C. The residue was reconstituted in 1 mL 5% distilled nitric acid. Samples were run on the Thermo Finnegan MC ICP-MS (Tomascak et al. 1999). A concentration check was performed on the samples and the blank to sample ratio was less than 10^{-3}, suggesting the samples were not contaminated during preparation. An L-SVEC standard were measured between each sample measurement. Lithium isotopic composition was calculated from the blank-corrected ration of $^{7}Li/^{6}Li$ divided by the average $^{7}Li/^{6}Li$ of the L-SVEC standard from before and after the sample. To calculate $\delta^{7}Li$, 1 was subtracted from this blank-corrected ratio and the final value was multiplied by 1000 and reported in ‰.In two out of three purification iterations, L-SVEC values were 0 +/– 0.5‰ and seawater values were 30 +/– 0.5‰. The percent error, which is less than 5% for both of these standards, suggests that 100% of lithium was recovered and that there was no fractionation in the mass spectrometer. L-SVEC was used to apply corrections when measured values deviated from 0‰.

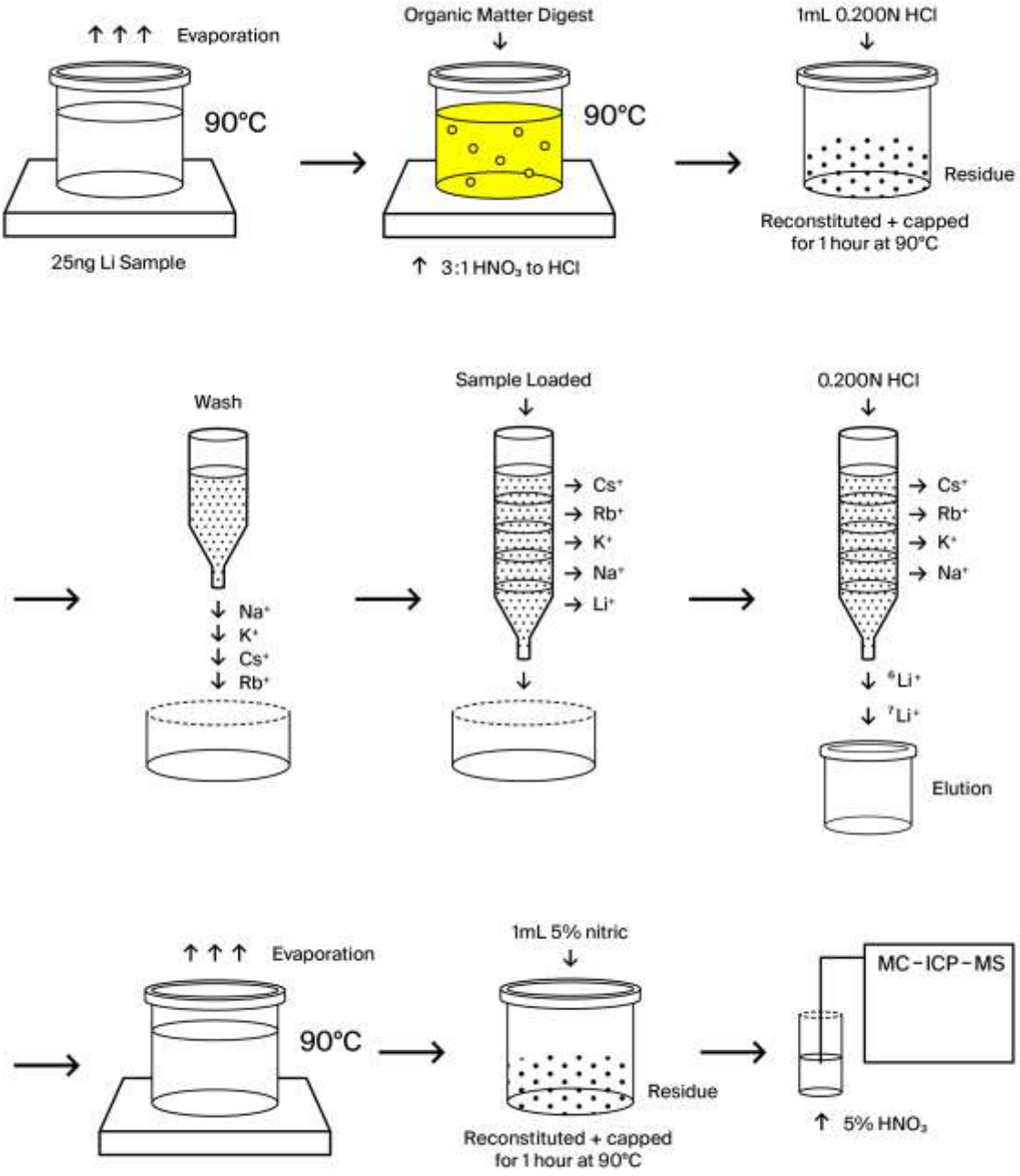

Figure 3: Methods for lithium isotope isolation and measurement.

RESULTS

Lithium Concentration:

The riverine lithium concentrations in this data set are not correlated with dominant bedrock lithology nor the geographic region of Thailand. Concentrations ranged from 0.024 μM to 0.788 μM, with a mean concentration of 0.140 μM (n = 67). This mean is lower than the global average of 0.32 μM (Gaillardet et al. 2014, Misra and Froelich 2012). The concentration of the Mekong, which has the largest discharge rate of all rivers sampled, was 0.207 μM, which is close to, but below, the global average lithium concentration in rivers. The concentration of the Chao Phraya River nearest the mouth was 0.106 μM, which is more dramatically lower than global averages.

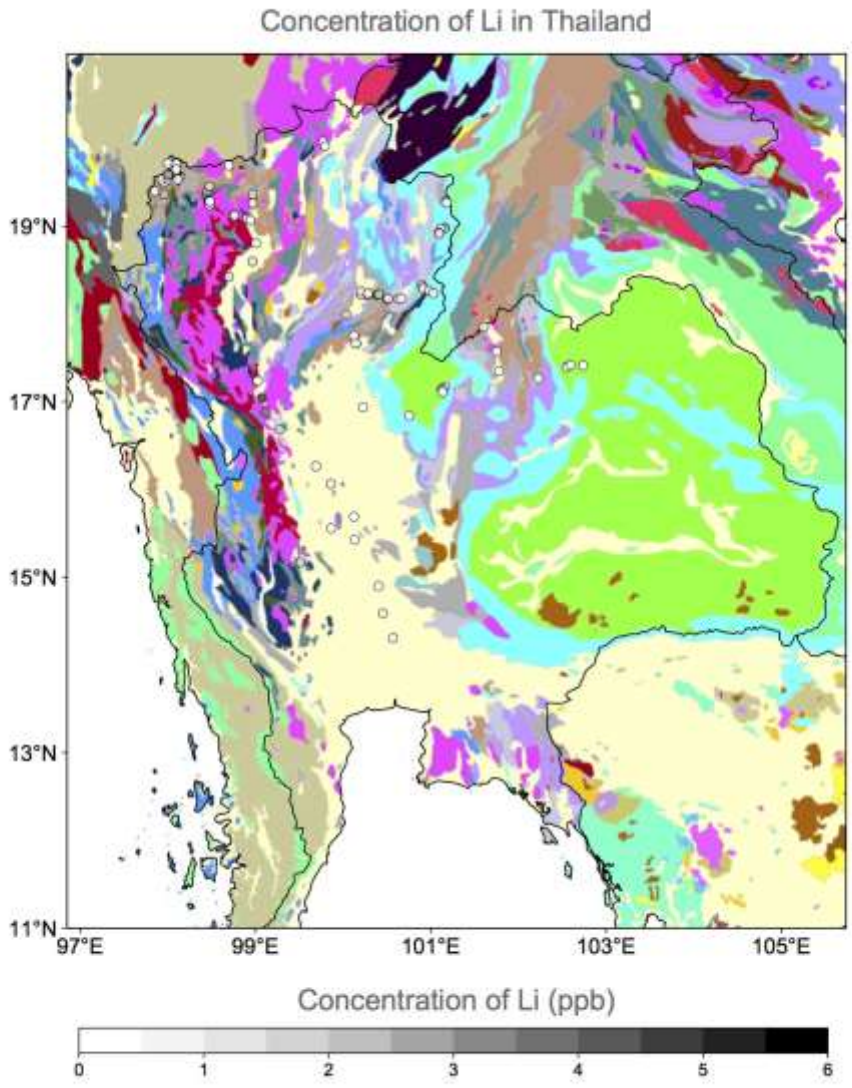

Figure 4: Concentration of river waters across a bedrock map of Thailand (see Appendix 1 for bedrock lithology key) map from OneGeology Portal

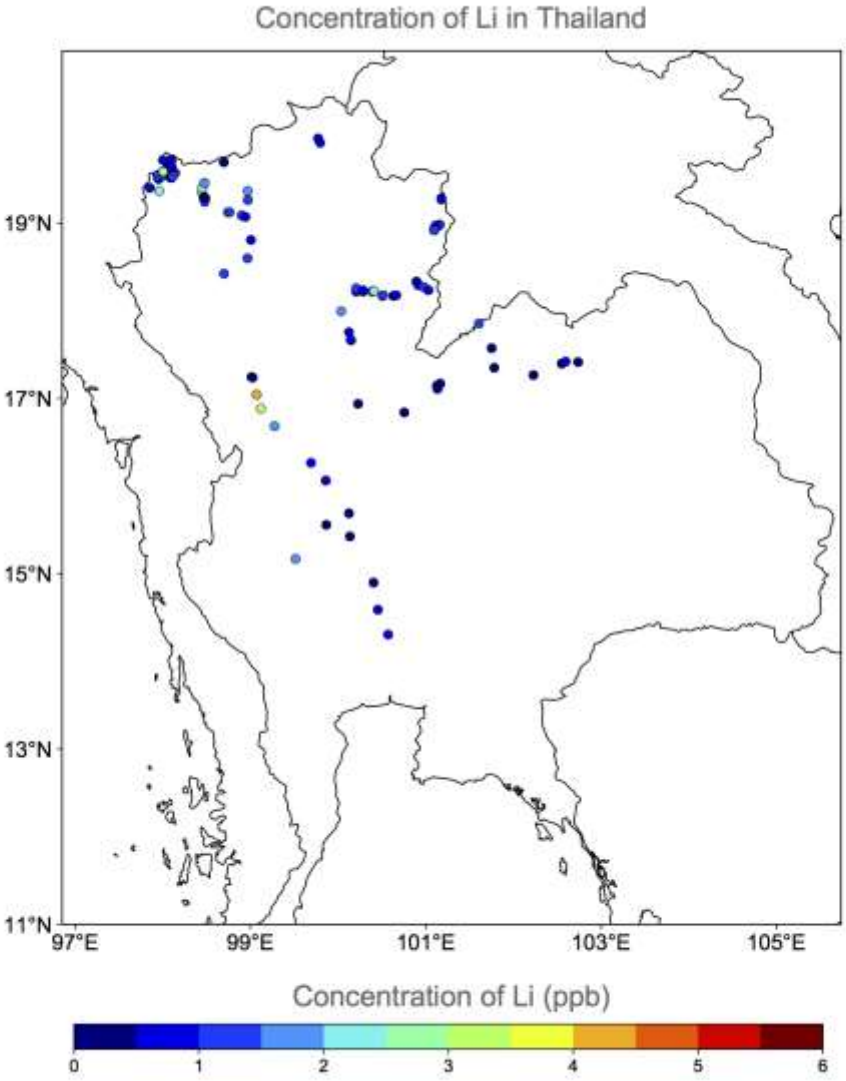

Figure 5: Concentration of river waters across Thailand by site location.

There was no significant association between lithium concentrations and the δ^7Li of the dissolved load. The δ^7Li ranged from –7.48‰ to 43.04‰. The average δ^7Li is 25.17‰, which is not far from the global average of 23‰ (Li and West 2014), although a large number of samples deviated markedly from the mean. Neither concentration nor elevation correlated with δ^7Li.

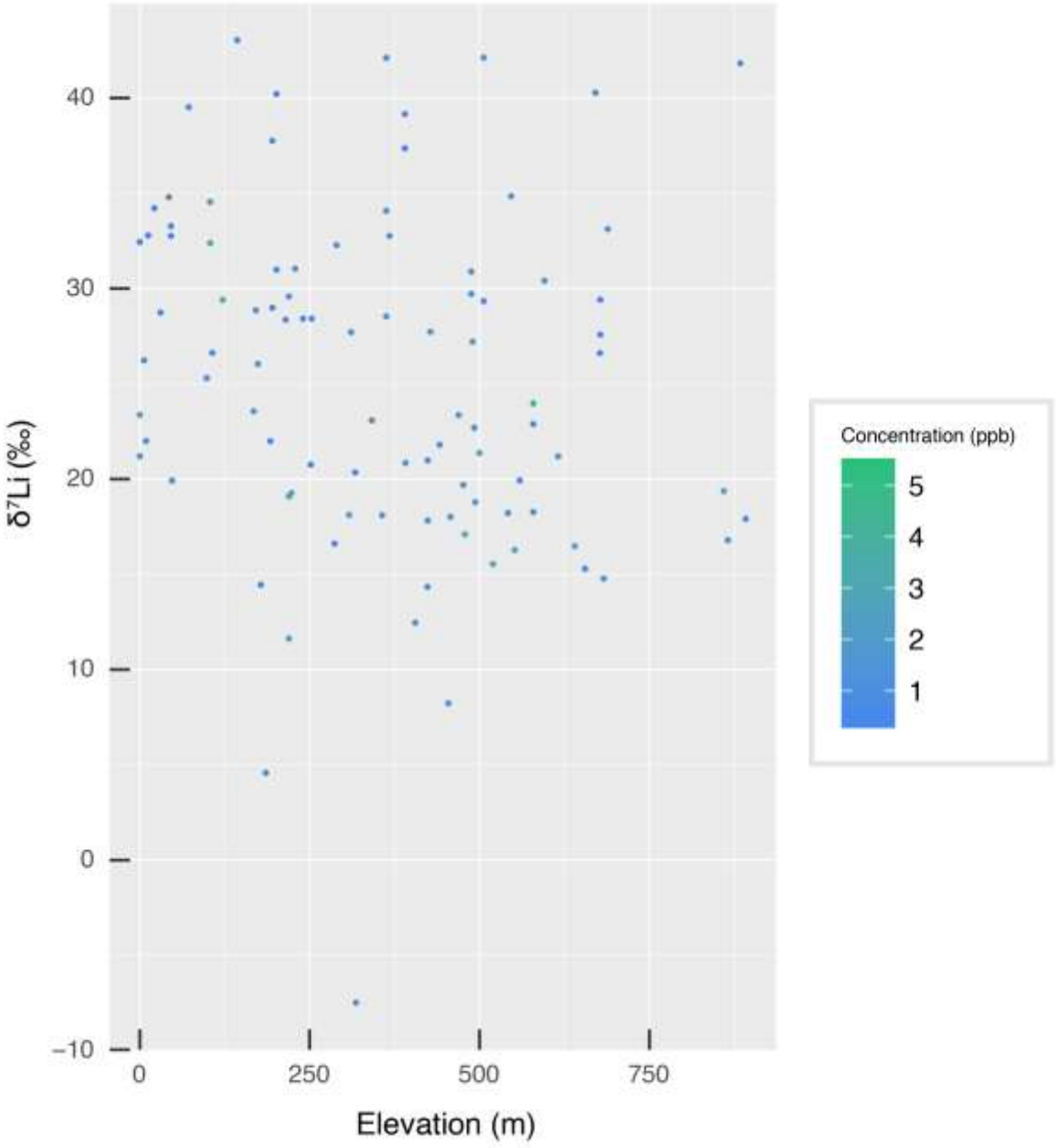

Figure 6: Lithium isotope fractionations plotted against concentration and elevation.

δ^7Li Values:

Extremely positive δ^7Li values were measured in all of the regions sampled.

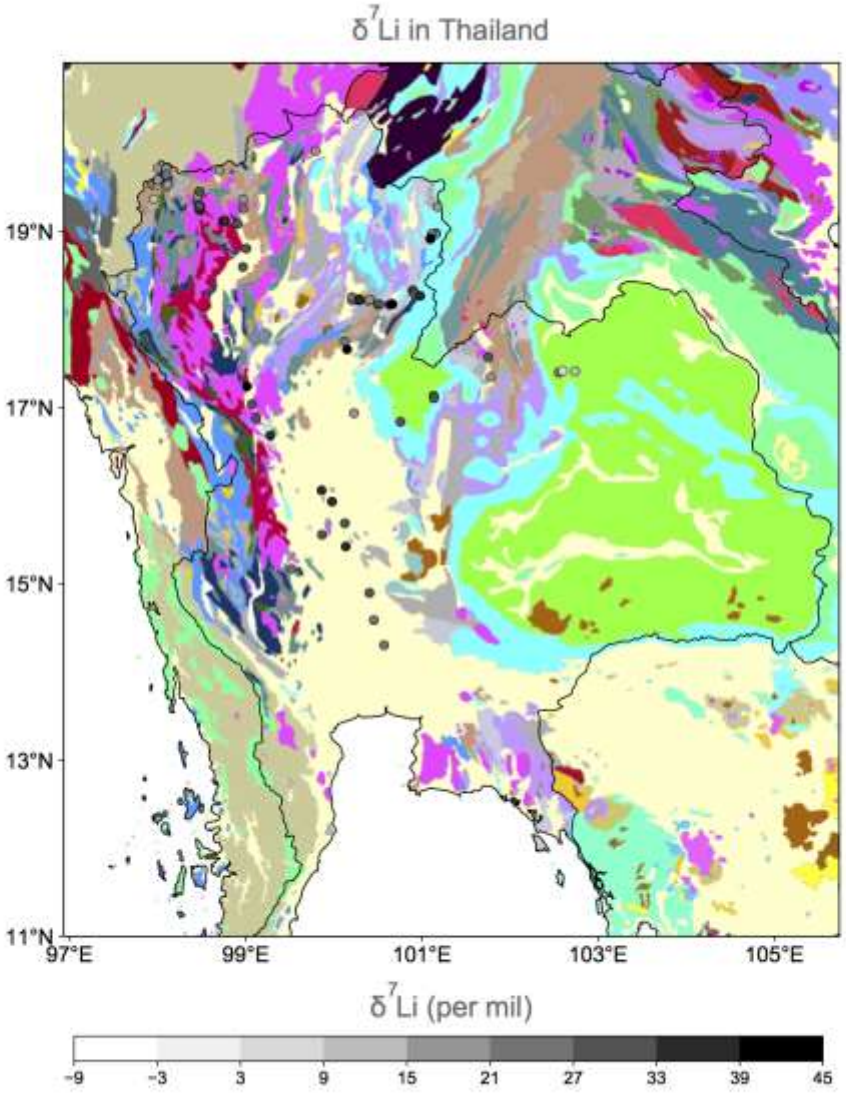

Figure 7: Lithium fractionations by site location on a bedrock lithological map (Map from OneGeology Portal)

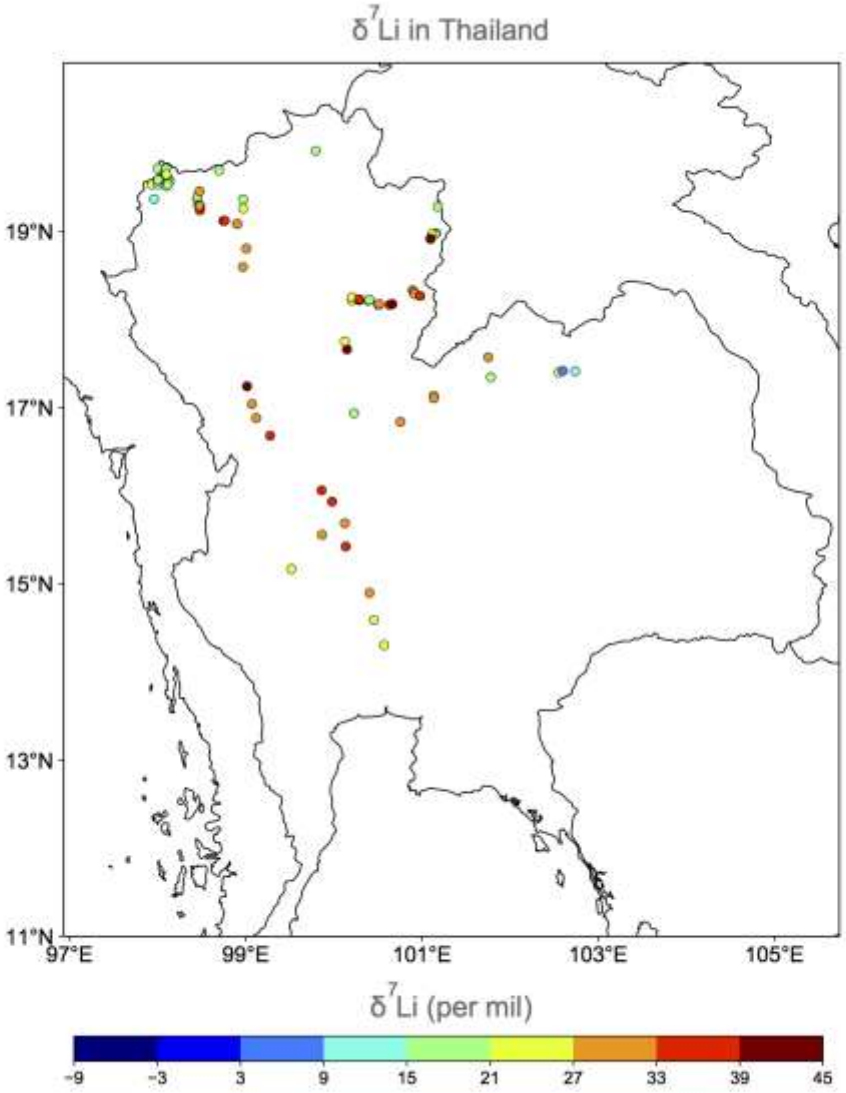

Figure 8: Lithium isotope fractionations by sample location

Time series:

Of the six rivers sampled during different weathering conditions, only one site had markedly different δ^7Li or concentration values (>10% difference) during different weather conditions. This suggests that storm events do not alter lithium concentrations or δ^7Li on short time scales. This is in line with existing evidence that large storm events do not cause short-term changes in lithium concentration or δ^7Li.

δ^7Li by River Size:

The δ^7Li values of samples were much more variable in small rivers. Mean δ^7Li for rivers by width category were as follows: 24.09‰ for rivers 1-3 m wide (n = 26), 24.92‰ for rivers 3-10 m wide (n = 25), 26.13‰ for rivers 10-100 m wide (n = 14) and 28.55‰ for rivers 100+ meters wide (n = 4).

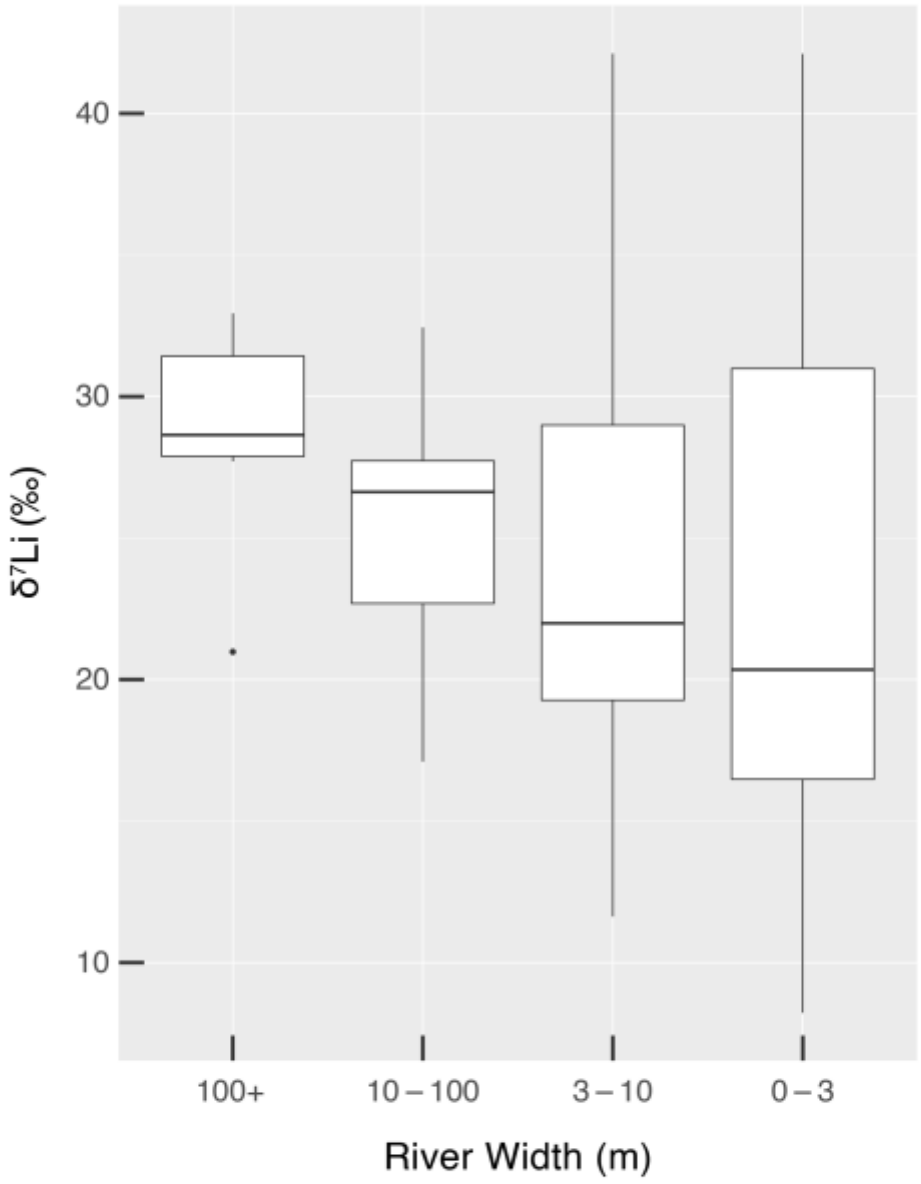

Figure 9: Median and standard deviations of dissolved load isotope values by river width

Silicate Weathering Flux:

The average concentration of silica was 0.0179 M, and the concentration of silica plus cations was 0.0652 M. The average sum of concentrations of silica and the cations magnesium (Mg), calcium (Ca) and sodium (Na) was 6.52 μM. In the Chao Phraya, the sum of the concentrations of cations (Na, Mg, Ca) and silica increased as latitude decreased, with the sum reaching a peak at 22.24 μM north of Greater Bangkok.

Carbonate Weathering:

The average percentage of lithium flux due to carbonate weathering was 5.9%, according to the calculation:

$$[Li]_{carb} = [Ca] * \left(\frac{Li}{Ca}\right)_{\text{carb}}$$

where the ratio of Li/Ca in carbonates was 1.5 x 10^{-5} (Hathorne & James 2006, Pogge von Strandmann et al. 2013).

DISCUSSION

These data broaden our understanding of both the range of environments with high δ^7Li inputs and the range of δ^7Li values that can be associated with regions of high silicate weathering rates. The mean δ^7Li value for all samples, 25.47‰, is within 10% of the 23‰ estimate for global river contributions to lithium isotope mass balance. Still, the average δ^7Li for large rivers, which make more meaningful contributions to seawater chemistry, was 28.5‰, which is much higher than river δ^7Li values in other regions of the world. To an extent, this is what we would expect. Thailand has much higher rates of chemical denudation than temperate and subarctic regions, so it makes sense that it would have a distinct isotopic contribution. However, the markedly different δ^7Li values in the Amazon, the mouth of which had a mean δ^7Li of 6.82‰, suggest existing interpretations for δ^7Li in regions with high chemical denudation rates must be reassessed (Dellinger et al. 2015).

The Amazon is a weathering regime we would expect to have similar rates of silicate weathering and clay formation — the pH of samples collected there was within 10% of the pH in this data set, and the mean annual temperatures and precipitation rates are both comparable to those of Thailand. Thus there must be some difference in clay formation in these regions that leads to the

markedly different δ^7Li values (Dellinger et al. 2015). One possibility is that it is not net precipitation, but instead precipitation patterns that determine the rates of clay formation. The wet and dry cycles of the Thai monsoon — on the order of several days — may lead to multiple clay formation events. One interpretation is that the intense rainfall leads to higher chemical dissolution rates by moving the river system away from saturation with respect to dissolved weathering products. Additionally, physical weathering rates may accelerate due to riverbed agitation from increased flow velocity and riverbank corasion associated with expansion of the surface area of the river bottom. The ensuing dry cycles then move the rivers towards saturation state, leading to precipitation of secondary clays and high δ^7Li values in the dissolved load. This is in line with models that have found that monsoon intensification in recent times has led to increased chemical denudation rates (Miriyala et al. 2017). Another possible factor that is not controlled for in our study, nor in the studies of the Amazon, is the stoichiometry of the specific clay minerals being formed — it is possible that the reaction rates of these clays differ and thus differential clay formation rates lead to differences in lithium withdrawal. Thus fractionation factors may need to be developed on a clay-by-clay basis.

Another factor that may distinguish the Amazon from Thailand is the rate of silicate weathering. The percentage of lithium input via silicate weathering in Thailand is on average 94.1%. This is lower than the percentage contribution of lithium from silicate weathering in the Amazon, which was consistently above 95%. Still, the concentration of silica, both alone and summed with cation concentrations, is 10-100 times greater in Thai rivers than it is in the Amazon sample sets. This suggests that silicate weathering productivity may be much higher in Thailand despite similarities in temperature, pH and precipitation. This is in line with other papers showing that the ratio of silicate weathering to other types of weathering is greater in Southeast Asia than it is in other parts of the world (Manaka et al. 2015). Since δ^7Li is supposed to track silicate weathering, it is promising that differences in silicate weathering fluxes yield different δ^7Li values. One explanation is that the high cation and dissolved silica concentrations in Thailand inhibit re-dissolution of secondary clays, or lead to higher rates of clay formation to begin with.

Regardless of the cause of variability across regions, this study shows that estimates for global riverine inputs that do not take into account the lithium flux from tropical systems during the monsoon season are incomplete. In the dissolved load alone, the Chao Phraya has a lithium flux

of 439.9 moles per year, and the Mekong has a lithium flux of 12,741 moles per year. While a small fraction of global riverine inputs ($10x10^9$ mol y^{-1}), these lithium isotope signatures have the potential to make meaningful impacts on seawater chemistry if this trend is matched in other parts of Southeast Asia. This also provides some insight to how weathering regime changes may have increased lithium values throughout the Cenozoic. A shift towards weathering regimes like Thailand, with dramatic swings in precipitation or unique clay species, may have occurred in regions like the Indian and African continents, which moved north into the ITCZ throughout the Cenozoic (van Hinsbergen et al 2012).

Unlike the Amazon Basin or the Ganges Alluvial Plain, δ^7Li values cannot be explained by elevation in this study (Pogge von Strandmann 2017, Dellinger et al. 2015). Here, both the highlands and lowlands contained δ^7Li greater than 33‰ along with several intermediate samples ranging between 15–21‰. Unlike the Ganges, which had remarkably constant δ^7Li values across different latitudes, the Chao Phraya, which begins in the lowlands at roughly 100 meters above sea level, experienced 12‰ variation throughout the main channel. There is likewise no association between δ^7Li and the ratio of Li/Na, Li/Mg or concentration as there has been in other studies (e.g. Millot et al. 2010, Dellinger et al. 2015, Pogge von Strandmann 2017). A negative correlation between the ratio of Li/Na and Li/Mg to the δ^7Li values has been interpreted as an indication that there was no fractionation during primary mineral dissolution (Millot et al. 2010). The lack of correlation across a much larger data set with similar weathering conditions suggests that this may not be a reliable way to discern fractionation during dissolution. The low rates of day-to-day variability among sites sampled during different weather conditions are in line with existing evidence that short-term weather patterns do not influence δ^7Li, which means future sampling should focus on sampling throughout different seasons to determine the effect of long-term weather patterns on δ^7Li.

Human influence on modern river Li

The high resolution of this data set also identifies several areas of potential human interference in modern rivers. Several samples were removed from analysis due to proximity to city centers, which increased the likelihood of trace metal overprinting from pollution. This was in part identified by a dramatic change in δ^7Li over short distance. The highest value observed (43‰) was from above a dam. Since samples of the same river in the same region but below the dam

were more than 10‰ lighter, it is possible that the build-up of sediments behind the dam provided more nucleation sites for ^{6}Li and, as a result, led to inflated $\delta^{7}Li$ values. The vast majority of the samples in this study were collected from rivers not subject to damming so dams did not contribute to the high variability in river isotope values that we observed. Still, this strong effect highlights the need to account for dams when examining lithium in modern systems.

SUMMARY

In summary, the $\delta^{7}Li$ values of Thailand's main rivers show that intense weathering regimes can produce high $\delta^{7}Li$ values. Many variables that explain $\delta^{7}Li$ values in other regions, such as concentration and elevation, do not explain the values seen in Thailand. The reason intense weathering can produce both high and low $\delta^{7}Li$ values may have to do with specific clay reaction dynamics or precipitation patterns. More broadly, these results highlight the need to improve our understanding of integrated $\delta^{7}Li$ and silicate weathering fluxes in Southeast Asia in order to apply lithium to the rock record.

FUTURE DIRECTIONS

In order to more thoroughly understand lithium behavior in this region of the world, further research is necessary both within this data set and within Southeast Asia. First, it is necessary to sample during the Thai dry season to provide an integrated estimate for annual lithium isotopic output. This will make it possible to determine how these positive $\delta^{7}Li$ values will translate into the rock record over thousands of years. Studies of Pacific Islands could isolate certain variables — like bedrock composition and elevation extent — while maintaining similar temperature and precipitation patterns. Higher sampling density across higher order rivers in Southeast Asia can also determine whether the progression towards $\delta^{7}Li$ values as river width increases holds across rivers that originate farther north in mainland Asia but pass through Southeast Asia before entering the Pacific.

This study focuses on the $\delta^{7}Li$ dissolved load, however, in order to fully understand lithium travelling through the rivers sampled, suspended load and river sediments must also be examined. This would give insight into riverine lithium sorting, since any isotopic fractionations in the dissolved load are likely off-set by fractionations in either the sediment pile or the

suspended load. It was initially thought that the suspended load — defined here as particles in the uppermost layers of the river that are greater than 2 μm in diameter — could be extracted from the 2 μm acetate cellulose filters used in the field. However, it became apparent that the filters could not be opened without introducing the risk of contamination from metal instruments or without losing parts of the sample. Since there would likely be a size-bias in sample dispersion, these measurements were not conducted. To include suspended load in this analysis, sediments could be collected from removable filters during sample collection. Suspended load could be categorized by ADCP (Acoustic Doppler Current Profiler) which quantifies flow-velocity, river depth and cross section, water discharge and heterogeneity of river turbidity (Dellinger et al. 2014). This would make it possible to control for environmental conditions in the analysis of suspended load compared to dissolved load. Using additional digestion steps, the suspended load and sediment samples could be isolated using the column procedure outlined in the materials and methods section and analyzed on the Thermo-Finnigen ICP-MS.

Additionally, an important question regarding dissolved lithium isotopic behavior is whether or not dissolved isotopic composition is conserved when rivers join. Since the discharge rates of most of the rivers sampled in this data set are not available due to their small size, discharge rates could be estimated using the surface area of river upstream to the sample site. From discharge rate and concentration, the δ^7Li flux could be calculated for each site. This could be used to determine whether or not the fractionation occurs before streams feed into larger rivers or if the isotopic fractionations observed are largely related to floodplain dynamics in these larger rivers.

ACKNOWLEDGEMENTS

Thank you first and foremost to Noah Planavsky for his guidance and teaching throughout the course of this project. Thank you to Ryan McKenzie for advice on the draft and for help with research design. Thank you to Guangyi Wei and Boriana Kalderon-Asael for help with lithium column chromatography and lithium concentration and isotope measurements and calculations. Thank you to Devon Cole, Jo Katchinoff, Cody Lee Colleps and Hyangyu Liu for help developing robust field methods and collecting samples. This work was made possible by the Karen Von Damm Fellowship and the Timothy Dwight College Mellon Grant.

REFERENCES

(2015). "The Li isotope response to mountain uplift." Geology 43(1): 67-70.

Brady, P. V. and S. A. Carroll (1994). "Direct effects of CO2 and temperature on silicate weathering: Possible implications for climate control." Geochimica et Cosmochimica Acta 58(7): 1853-1856.

Brady, P. V., R. I. Dorn, A. J. Brazel, J. Clark, R. B. Moore and T. Glidewell (1999). "Direct measurement of the combined effects of lichen, rainfall, and temperature onsilicate weathering." Geochimica et Cosmochimica Acta 63(19): 3293-3300.

Brady, P. V., R. I. Dorn, A. J. Brazel, J. Clark, R. B. Moore and T. Glidewell (1999). "Direct measurement of the combined effects of lichen, rainfall, and temperature onsilicate weathering." Geochimica et Cosmochimica Acta 63(19): 3293-3300.

Dellinger, M., J. Bouchez, J. Gaillardet, L. Faure and J. Moureau (2017). "Tracing weathering regimes using the lithium isotope composition of detrital sediments." Geology 45(5): 411-414.

Dellinger, M., J. Gaillardet, J. Bouchez, D. Calmels, V. Galy, R. G. Hilton, P. Louvat and C. France-Lanord (2014). "Lithium isotopes in large rivers reveal the cannibalistic nature of modern continental weathering and erosion." Earth and Planetary Science Letters 401: 359-372.

Dellinger, M., J. Gaillardet, J. Bouchez, D. Calmels, V. Galy, R. G. Hilton, P. Louvat and C. France-Lanord (2014). "Lithium isotopes in large rivers reveal the cannibalistic nature of modern continental weathering and erosion." Earth and Planetary Science Letters 401: 359-372.

Froelich, F. and S. Misra (2014). "Was the Late Paleocene-Early Eocene Hot Because Earth Was Flat?

Froelich, M.S. and Misra, S. A. An Ocean Lithium Isotope View of Mountain Building, Continental Weathering, Carbon Dioxide, and Earth's Cenozoic Climate." Oceanography 27(1): 36-49.

Gaillardet, J., B. Dupré, P. Louvat and C. J. Allègre (1999). "Global silicate weathering and CO2 consumption rates deduced from the chemistry of large rivers." Chemical Geology 159(1): 3-30.

Global River Discharge Database. The University of Wisconsin Hydrological Institute. Url: https://nelson.wisc.edu/sage/data-and-models/riverdata/

Hartmann, J., N. Moosdorf, R. Lauerwald, M. Hinderer and A. J. West (2014). "Global chemical weathering and associated P-release — The role of lithology, temperature and soil properties." Chemical Geology 363: 145-163.

Hathorne, E. C. and R. H. James (2006). "Temporal record of lithium in seawater: A tracer for silicate weathering?" Earth and Planetary Science Letters 246(3): 393-406.

Henchiri, S., J. Gaillardet, M. Dellinger, J. Bouchez and G. M. Spencer Robert (2016). "Riverine dissolved lithium isotopic signatures in low‐relief central Africa and their link to weathering regimes." Geophysical Research Letters 43(9): 4391-4399.

Hodell, D. A., P. A. Mueller and J. R. Garrido (1991). Strontium isotopic composition and chronology of sediments from DSDP Site 90-588, PANGAEA.

James, R. H. and M. R. Palmer (2000). "The lithium isotope composition of international rock standards." Chemical Geology 166(3): 319-326.

Jamrussri, S. and Y. Toda (2017). "Simulating past severe flood events to evaluate the effectiveness of nonstructural flood countermeasures in the upper Chao Phraya River Basin, Thailand." Journal of Hydrology: Regional Studies 10: 82-94.

Li, G. and A. J. West (2014). "Evolution of Cenozoic seawater lithium isotopes: Coupling of global denudation regime and shifting seawater sinks." Earth and Planetary Science Letters 401: 284-293.

Manaka, T., S. Otani, A. Inamura, A. Suzuki, T. Aung, R. Roachanakanan, T. Ishiwa and H. Kawahata (2015). "Chemical weathering and long‐term CO2 consumption in the Ayeyarwady and Mekong river basins in the Himalayas." Journal of Geophysical Research: Biogeosciences 120(6): 1165-1175.

Misra, S. and P. N. Froelich (2012). "Lithium Isotope History of Cenozoic Seawater: Changes in Silicate Weathering and Reverse Weathering." Science 335(6070): 818.

Meteorological Department, (2001): Climatological Data of Thailand. 1951-2001. url: http://hywr.kuciv.kyoto-u.ac.jp/ihp/riverCatalogue/Vol_05/10_Thailand-12.pdf

Moriguti, T. and E. Nakamura (1998). "High-yield lithium separation and the precise isotopic analysis for natural rock and aqueous samples." Chemical Geology 145(1): 91-104.

Oi, T., T. Odagiri and M. Nomura (1997). "Extraction of lithium from GSJ rock reference samples and determination of their lithium isotopic compositions." Analytica Chimica Acta 340(1): 221-225.

One Geology Portal: http://www.onegeology.org/service_provision/onegeology_profile.html

Peucker‐Ehrenbrink, B. and G. Ravizza (2002). "The marine osmium isotope record." Terra Nova 12(5): 205-219.

Schmitt, A.-D., N. Vigier, D. Lemarchand, R. Millot, P. Stille and F. Chabaux (2012). "Processes controlling the stable isotope compositions of Li, B, Mg and Ca in plants, soils and waters: A review." Comptes Rendus Geoscience 344(11): 704-722.

Tang, Y.-J., H.-F. Zhang and J.-F. Ying (2007). "Review of the Lithium Isotope System as a Geochemical Tracer." International Geology Review 49(4): 374-388.

Taylor, T. I. and H. C. Urey (1938). "Fractionation of the Lithium and Potassium Isotopes by Chemical Exchange with Zeolites." The Journal of Chemical Physics 6(8): 429-438.

van Hinsbergen, D. J. J., P. C. Lippert, G. Dupont-Nivet, N. McQuarrie, P. V. Doubrovine, W. Spakman and T. H. Torsvik (2012). "Greater India Basin hypothesis and a two-stage Cenozoic collision between India and Asia." Proceedings of the National Academy of Sciences 109(20): 7659.

Vigier, N., S. R. Gislason, K. W. Burton, R. Millot and F. Mokadem (2009). "The relationship between riverine lithium isotope composition and silicate weathering rates in Iceland." Earth and Planetary Science Letters 287(3): 434-441.

von Strandmann, P., P. J. Frings and M. J. Murphy (2017). "Lithium isotope behaviour during weathering in the Ganges Alluvial Plain." Geochimica Et Cosmochimica Acta 198: 17-31.

Wang, Q.-L., B. Chetelat, Z.-Q. Zhao, H. Ding, S.-L. Li, B.-L. Wang, J. Li and X.-L. Liu (2015). "Behavior of lithium isotopes in the Changjiang River system: Sources effects and response to weathering and erosion." Geochimica et Cosmochimica Acta 151: 117-132.

Wang, Q.-L., B. Chetelat, Z.-Q. Zhao, H. Ding, S.-L. Li, B.-L. Wang, J. Li and X.-L. Liu (2015). "Behavior of lithium isotopes in the Changjiang River system: Sources effects and response to weathering and erosion." Geochimica et Cosmochimica Acta 151: 117-132.

Weynell, M., U. Wiechert and J. A. Schuessler (2017). "Lithium isotopes and implications on chemical weathering in the catchment of Lake Donggi Cona, northeastern Tibetan Plateau." Geochimica Et Cosmochimica Acta 213: 155-177.

Zachos, J., M. Pagani, L. Sloan, E. Thomas and K. Billups (2001). "Trends, Rhythms, and Aberrations in Global Climate 65 Ma to Present." Science 292(5517): 686.

Zachos, J. C., U. Röhl, S. A. Schellenberg, A. Sluijs, D. A. Hodell, D. C. Kelly, E. Thomas, M. Nicolo, I. Raffi, L. J. Lourens, H. McCarren and D. Kroon (2005). "Rapid Acidification of the Ocean During the Paleocene-Eocene Thermal Maximum." Science 308(5728): 1611.

Pogge von Strandmann & Henderson (2015). "The Li isotope response to mountain uplift." Geology 43(1): 67-70.

APPENDIX

Legend for OneGeology Portal Bedrock Map

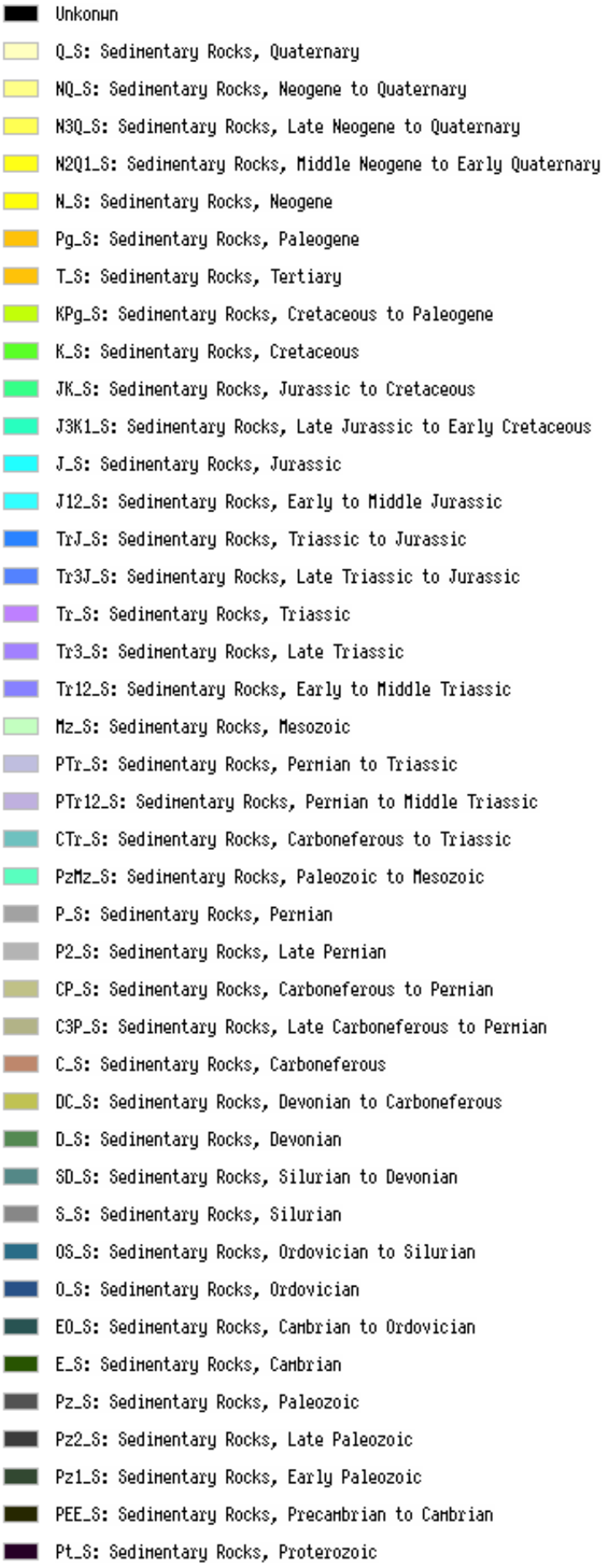
Unkonun
Q_S: Sedimentary Rocks, Quaternary
NQ_S: Sedimentary Rocks, Neogene to Quaternary
N3Q_S: Sedimentary Rocks, Late Neogene to Quaternary
N2Q1_S: Sedimentary Rocks, Middle Neogene to Early Quaternary
N_S: Sedimentary Rocks, Neogene
Pg_S: Sedimentary Rocks, Paleogene
T_S: Sedimentary Rocks, Tertiary
KPg_S: Sedimentary Rocks, Cretaceous to Paleogene
K_S: Sedimentary Rocks, Cretaceous
JK_S: Sedimentary Rocks, Jurassic to Cretaceous
J3K1_S: Sedimentary Rocks, Late Jurassic to Early Cretaceous
J_S: Sedimentary Rocks, Jurassic
J12_S: Sedimentary Rocks, Early to Middle Jurassic
TrJ_S: Sedimentary Rocks, Triassic to Jurassic
Tr3J_S: Sedimentary Rocks, Late Triassic to Jurassic
Tr_S: Sedimentary Rocks, Triassic
Tr3_S: Sedimentary Rocks, Late Triassic
Tr12_S: Sedimentary Rocks, Early to Middle Triassic
Mz_S: Sedimentary Rocks, Mesozoic
PTr_S: Sedimentary Rocks, Permian to Triassic
PTr12_S: Sedimentary Rocks, Permian to Middle Triassic
CTr_S: Sedimentary Rocks, Carboneferous to Triassic
PzMz_S: Sedimentary Rocks, Paleozoic to Mesozoic
P_S: Sedimentary Rocks, Permian
P2_S: Sedimentary Rocks, Late Permian
CP_S: Sedimentary Rocks, Carboneferous to Permian
C3P_S: Sedimentary Rocks, Late Carboneferous to Permian
C_S: Sedimentary Rocks, Carboneferous
DC_S: Sedimentary Rocks, Devonian to Carboneferous
D_S: Sedimentary Rocks, Devonian
SD_S: Sedimentary Rocks, Silurian to Devonian
S_S: Sedimentary Rocks, Silurian
OS_S: Sedimentary Rocks, Ordovician to Silurian
O_S: Sedimentary Rocks, Ordovician
EO_S: Sedimentary Rocks, Cambrian to Ordovician
E_S: Sedimentary Rocks, Cambrian
Pz_S: Sedimentary Rocks, Paleozoic
Pz2_S: Sedimentary Rocks, Late Paleozoic
Pz1_S: Sedimentary Rocks, Early Paleozoic
PEE_S: Sedimentary Rocks, Precambrian to Cambrian
Pt_S: Sedimentary Rocks, Proterozoic


Q_Vf: Felsic Volcanic Rocks, Quaternary
Q_Vfi: Felsic to Intermediate Volcanic Rocks, Quaternary
Q_Vi: Intermediate Volcanic Rocks, Quaternary
Q_Vim: Intermediate to Mafic Volcanic Rocks, Quaternary
Q_Vm: Mafic Volcanic Rocks, Quaternary
Q_Vu: Volcanic Rocks of Unknown Composition, Quaternary
NQ_Vfi: Felsic to Intermediate Volcanic Rocks, Neogene to Quaternary
NQ_Vi: Intermediate Volcanic Rocks, Neogene to Quaternary
NQ_Vim: Intermediate to Mafic Volcanic Rocks, Neogene to Quaternary
NQ_Vm: Mafic Volcanic Rocks, Neogene to Quaternary
N_Vf: Felsic Volcanic Rocks, Neogene
N_Vfi: Felsic to Intermediate Volcanic Rocks, Neogene
N_Vi: Intermediate Volcanic Rocks, Neogene
N_Vim: Intermediate to Mafic Volcanic Rocks, Neogene
N_Vm: Mafic Volcanic Rocks, Neogene
N_Vu: Volcanic Rocks of Unknown Composition, Neogene
Pg_Vf: Felsic Volcanic Rocks, Paleogene
Pg_Vfi: Felsic to Intermediate Volcanic Rocks, Paleogene
Pg_Vim: Intermediate to Mafic Volcanic Rocks, Paleogene
Pg_Vm: Mafic Volcanic Rocks, Paleogene
T_Vf: Felsic Volcanic Rocks, Tertiary
T_Vfi: Felsic to Intermediate Volcanic Rocks, Tertiary
T_Vim: Intermediate to Mafic Volcanic Rocks, Tertiary
Cz_Vm: Mafic Volcanic Rocks, Cenozoic
KPg_Vf: Felsic Volcanic Rocks, Cretaceous to Paleogene
K_Vf: Felsic Volcanic Rocks, Cretaceous
K_Vfi: Felsic Volcanic Rocks, Cretaceous
K_Vi: Intermediate Volcanic Rocks, Cretaceous
K_Vm: Mafic Volcanic Rocks, Cretaceous
JK_Vi: Intermediate Volcanic Rocks, Jurassic to Cretaceous
JK_Vm: Mafic Volcanic Rocks, Jurassic to Cretaceous
J3K_Vi: Intermediate Volcanic Rocks, Late Jurassic to Cretaceous
J_Vf: Felsis Volcanic Rocks, Jurassic
J_Vfi: Felsic to Intermediate Volcanic Rocks, Jurassic
J_Vi: Intermediate Volcanic Rocks, Jurassic
J_Vim: Intermediate to Mafic Volcanic Rocks, Jurassic
J_Vm: Mafic Volcanic Rocks, Jurassic
Tr_Vf: Felsic Volcanic Rocks, Triassic
Tr_Vi: Intermediate Volcanic Rocks, Triassic
Tr_Vim: Intermediate to Mafic Volcanic Rocks, Triassic
Mz_Vf: Felsic Volcanic Rocks, Mesozoic

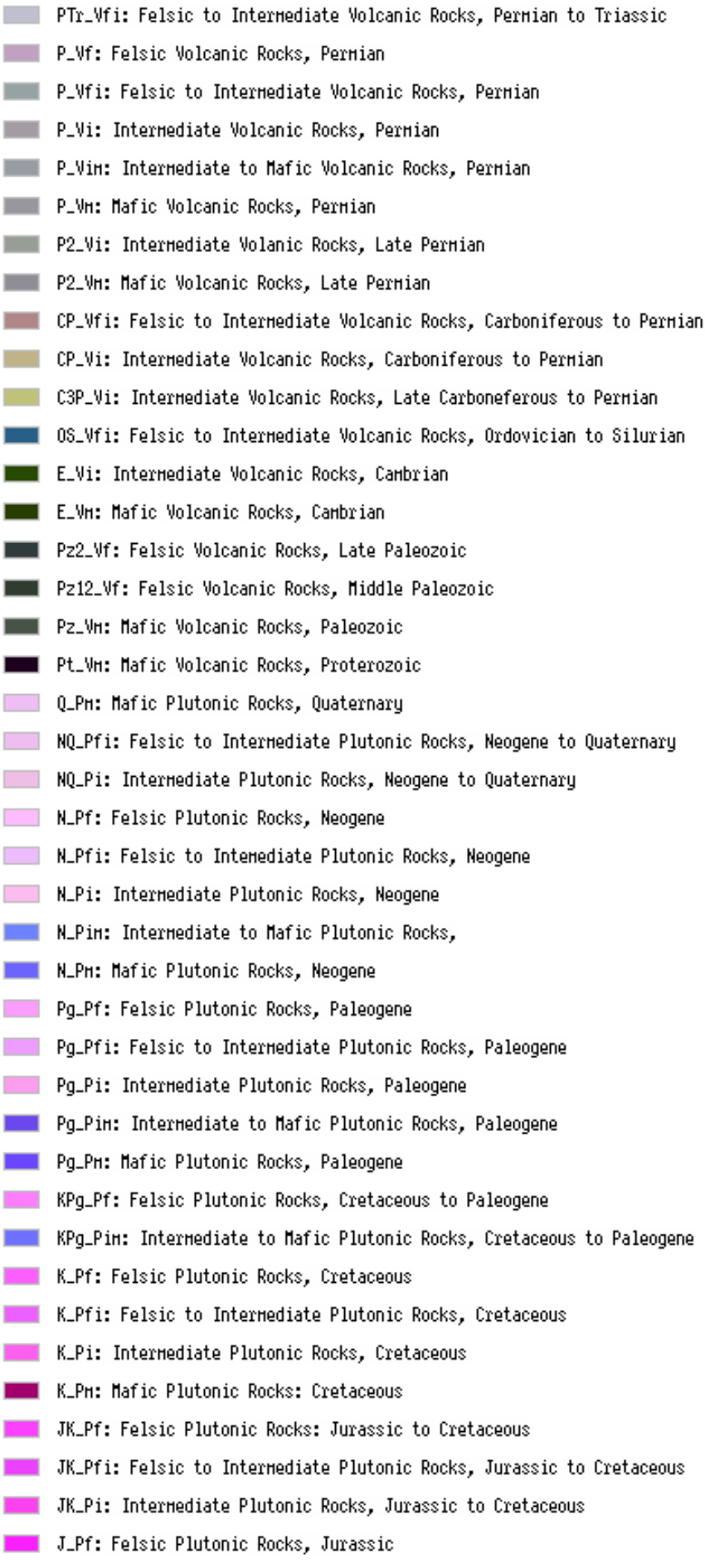
PTr_Vfi: Felsic to Intermediate Volcanic Rocks, Permian to Triassic
P_Vf: Felsic Volcanic Rocks, Permian
P_Vfi: Felsic to Intermediate Volcanic Rocks, Permian
P_Vi: Intermediate Volcanic Rocks, Permian
P_Vim: Intermediate to Mafic Volcanic Rocks, Permian
P_Vm: Mafic Volcanic Rocks, Permian
P2_Vi: Intermediate Volanic Rocks, Late Permian
P2_Vm: Mafic Volcanic Rocks, Late Permian
CP_Vfi: Felsic to Intermediate Volcanic Rocks, Carboniferous to Permian
CP_Vi: Intermediate Volcanic Rocks, Carboniferous to Permian
C3P_Vi: Intermediate Volcanic Rocks, Late Carboneferous to Permian
OS_Vfi: Felsic to Intermediate Volcanic Rocks, Ordovician to Silurian
E_Vi: Intermediate Volcanic Rocks, Cambrian
E_Vm: Mafic Volcanic Rocks, Cambrian
Pz2_Vf: Felsic Volcanic Rocks, Late Paleozoic
Pz12_Vf: Felsic Volcanic Rocks, Middle Paleozoic
Pz_Vm: Mafic Volcanic Rocks, Paleozoic
Pt_Vm: Mafic Volcanic Rocks, Proterozoic
Q_Pm: Mafic Plutonic Rocks, Quaternary
NQ_Pfi: Felsic to Intermediate Plutonic Rocks, Neogene to Quaternary
NQ_Pi: Intermediate Plutonic Rocks, Neogene to Quaternary
N_Pf: Felsic Plutonic Rocks, Neogene
N_Pfi: Felsic to Intemediate Plutonic Rocks, Neogene
N_Pi: Intermediate Plutonic Rocks, Neogene
N_Pim: Intermediate to Mafic Plutonic Rocks,
N_Pm: Mafic Plutonic Rocks, Neogene
Pg_Pf: Felsic Plutonic Rocks, Paleogene
Pg_Pfi: Felsic to Intermediate Plutonic Rocks, Paleogene
Pg_Pi: Intermediate Plutonic Rocks, Paleogene
Pg_Pim: Intermediate to Mafic Plutonic Rocks, Paleogene
Pg_Pm: Mafic Plutonic Rocks, Paleogene
KPg_Pf: Felsic Plutonic Rocks, Cretaceous to Paleogene
KPg_Pim: Intermediate to Mafic Plutonic Rocks, Cretaceous to Paleogene
K_Pf: Felsic Plutonic Rocks, Cretaceous
K_Pfi: Felsic to Intermediate Plutonic Rocks, Cretaceous
K_Pi: Intermediate Plutonic Rocks, Cretaceous
K_Pm: Mafic Plutonic Rocks: Cretaceous
JK_Pf: Felsic Plutonic Rocks: Jurassic to Cretaceous
JK_Pfi: Felsic to Intermediate Plutonic Rocks, Jurassic to Cretaceous
JK_Pi: Intermediate Plutonic Rocks, Jurassic to Cretaceous
J_Pf: Felsic Plutonic Rocks, Jurassic


J_Pfi: Felsic to Intermediate Plutonic Rocks, Jurassic
J_Pi: Intermediate Plutonic Rocks, Jurassic
J_Pm: Mafic Plutonic Rocks, Jurassic
TrJ_Pf: Felsic Plutonic Rocks, Triassic to Jurassic
Tr_Pf: Felsic Plutonic Rocks, Triassic
Tr_Pfi: Felsic to Intermediate Plutonic Rocks, Triassic
Tr_Pi: Intermediate Plutonic Rocks, Triassic
Tr_Pm: Mafic Plutonic Rocks, Triassic
Mz_Pf: Felsic Plutonic Rocks, Mesozoic
Mz_Pfi: Felsic to Intermediate Plutonic Rocks, Mesozoic
Mz_Pi: Intermediate Plutonic Rocks, Mesozoic
Mz_Pm: Mafic Plutonic Rocks, Mesozoic
PTr_Pf: Felsic Plutonic Rocks, Permian to Triassic
P_Pf: Felsic Plutonic Rocks, Permian
P_Pfi: Felsic to Intermediate Plutonic Rocks, Permian
P_Pi: Intermediate Plutonic Rocks, Permian
P_Pm: Mafic Plutonic Rocks, Permian
Pz2_Pf: Felsic Plutonic Rocks, Late Paleozoic
Pz2_Pfi: Felsic to Intermediate Plutonic Rocks, Late Paleozoic
Pz2_Pi: Intermediate Plutonic Rocks, Late Paleozoic
Pz2_Pm: Mafic Plutonic Rocks, Late Paleozoic
Pz12_Pf: Felsic Plutonic Rocks, Middle Paleozoic
Pz12_Pu: Plutonic Rocks of Unknown Composition, Middle Paleozoic
Pz1_Pf: Felsic Plutonic Rocks, Early Paleozoic
Pz1_Pi: Intermediate Plutonic Rocks, Early Paleozoic
Pz1_Pm: Mafic Plutonic Rocks, Early Paleozoic
Pz_Pf: Felsic Plutonic Rocks, Paleozoic
Pt3_Pf: Felsic Plutonic Rocks, Late Proterozoic
Pt_Pf: Felsic Plutonic Rocks, Proterozoic
Pt_Pfi: Felsic to Intermediate Plutonic Rocks, Proterozoic
Pt_Pm: Mafic Plutonic Rocks, Proterozoic
APt_Pf: Felsic Plutonic Rocks, Archean to Proterozoic
A_Pf: Felsic Plutonic Rocks, Archean
A_Pi: Intermediate Plutonic Rocks, Archean
A_Pm: Mafic Plutonic Rocks, Archean
PE_Pf: Felsic Plutonic Rocks, Precambrian
Uk_Pf: Felsic Plutonic Rocks, Unknown Age
Uk_Pm: Mafic Plutonic Rocks, Unknown Age
Uk_Pu: Plutonic Rocks of Unknown Composition, Unknown Age
Pg_Mi: Intermediate Grade Metamorphic Rocks, Paleogene
K_Mi: Intermediate Grade Metamorphic Rocks, Cretaceous
J_Mi: Intermediate Grade Metamorphic Rocks, Jurassic


Tr_Mi: Intermediate Grade Metamorphic Rocks, Triassic
Tr_Mu: Metamorphic Rocks of Unknown Grade, Triassic
Mz_Ml: Low Grade Metamorphic Rocks, Mesozoic
P_Mi: Intermediate Grade Metamorphic Rocks, Permian
P_Mu: Metamorphic Rocks of Unknown Grade, Permian
CP_Mu: Metamorphic Rocks of Unknown Grade, Carboniferous to Permian
C_Mi: Intermediate Metamorphic Rocks, Carboneferous
C_Mu: Metamorphic Rocks of Unknown Grade, Carboneferous
D_Mu: Metamorphic Rocks of Unknown Grade, Devonian
SD_Ml: Law Grade Metamorphic Rocks, Silurian to Devonian
S_Ml: Low Grade Metamorphic Rocks, Silurian
OS_Mu: Low Grade Metamorphic Rocks, Ordovician to Silurian
O_Ml: Low Grade Metamorphic Rocks, Ordovician
EO_Ml: Low Grade Metamorphic Rocks, Cambrian to Ordovician
E_Mu: Metamorphic Rocks of Unknown Grade, Cambrian
Pz1_Mi: Intermediate Grade Metamorphic Rocks, Early Paleozoic
Pz_Mi: Intermediate Grade Metamorphic Rocks, Paleozoic
Pz_Ml: Low Grade Metamorphic Rocks, Paleozoic
Pz_Mu: Metamorphic Rocks of Unknown Grade, Paleozoic
Pt3_Mi: Intermediate Grade Metamorphic Rocks, Late Proterozoic
Pt3_Ml: Low Grade Metamorphic Rocks, Late Proterozoic
Pt2_Mi: Intermediate Grade Metamorphic Rocks, Middle Proterozoic
Pt2_Ml: Low Grade Metamorphic Rocks, Middle Proterozoic
Pt1_Mh: High Grade Metamorphic Rocks, Early Proterozoic
Pt1_Mi: Intermediate Grade Metamorphic Rocks, Early Proterozoic
Pt1_Ml: Low Grade Metamorphic Rocks, Early Proterozoic
Pt_Mh: High Grade Metamorphic Rocks, Proterozoic
Pt_Mi: Intermediate Grade Metamorphic Rocks, Proterozoic
Pt_Ml: Low Grade Metamorphic Rocks, Proterozoic
Pt_Mu: Metamorphic Rocks of Unknown Grade, Proterozoic
A_Mh: High Grade Metamorphic Rocks, Archean
A_Mi: Intermediate Grade Metamorphic Rocks, Archean
A_Ml: Low Grade Metamorphic Rocks, Archean
PE_Mh: High Grade Metamorphic Rocks, Precambrian
PE_Mi: Intermediate Grade Metamorphic Rocks, Precambrian
PE_Ml: Low Grade Metamorphic Rocks, Precambrian
PE_Mu: Metamorphic Rocks of Unknown Grade, Precambrian
U: Ultramafic Rocks
Water